INFLUENCE OF POROUS DAMAGE ON FATIGUE CRACK GROWTH

ER, Sérgio[1*]; FV, Ventura[1]; DM, Neto[1]

[1] Centre for Mechanical Engineering, Materials and Processes (CEMMPRE).
Department of Mechanical Engineering. University of Coimbra.
R. Luis Reis dos Santos 290, 3030-194 Coimbra
Persona de contacto: edmundo.sergio@uc.pt

RESUMEN

La fatiga es el resultado de la aparición de varios mecanismos de daño y sus interacciones. Por lo tanto, comprender cada mecanismo y las interacciones entre estos es crucial para modelar el proceso de crecimiento de grieta por fatiga (FCG). En este trabajo se considera que la deformación plástica cíclica, en el vértice de la grieta, es la fuerza impulsora del FCG. Se utiliza un modelo de daño GTN para tener en cuenta la degradación del material debido a la acumulación de porosidad. En el caso del aluminio 2024-T351, los resultados muestran una aproximación de las predicciones numéricas a los datos experimentales al introducir el daño poroso. Se discuten las razones detrás de esta aproximación, mostrándose que el daño poroso influye directamente en el cierre de grieta y en los resultados *da/dN*.

PALABRAS CLAVE: Crecimiento de Fendas por Fatiga, Fatiga, Deformación Plástica, Daño Porosos

ABSTRACT

Fatigue results from the occurrence of several damage mechanisms and their interactions. Therefore, the understanding of each mechanism and how it affects the others is crucial to model the fatigue crack growth (FCG) process. In this work the cyclic plastic strain, at the crack tip, is considered to be the FCG driving force. The GTN damage model is used to account for the material degradation due to the accumulation of porosity. For the 2024-T351 aluminium alloy, the results show an approximation of the numeric predictions to the experimental data by introducing porous damage. The reasons behind this approximation are discussed, being shown that porous damage directly influences crack closure and the *da/dN* results.

KEYWORDS: Fatigue Crack Growth, Plastic Strain, Porous Damage

1. INTRODUCTION

Fatigue is one of the main failure causes in mechanical operating devices. It is usually related with the occurrence of defects, which may evolve into cracks. These defects are inevitable in several material processing methods, such as welding, casting [1] and addictive manufacturing [2]. Being hard to obtain defect-free components, the damage tolerance approach has become a common way to deal with the fatigue phenomenon in industry. However, this approach requires the ability to predict the fatigue crack growth (FCG) rate, which has been mainly achieved through the stress intensity factor range (ΔK). This parameter is generally used to obtain correlations with experimental results, originating the so-called *da/dN*-ΔK curves. In fact, the parameter ΔK is involved in several useful crack growth laws, probably the most famous being Paris' law [3]. However, this parameter proved to be constrained to the Small-Scale Yielding (SSY) condition [4] and unable to characterise various fatigue phenomena. Indeed, ΔK fails to predict the effect of stress ratio, variable amplitude loading and the odd behaviour observed in short cracks [5]. These limitations urged the introduction of non-linear crack-tip parameters [6–8].
Furthermore, several models enclosing crack closure and considering the plastic strain, at the crack tip, as fatigue driving force provided FCG predictions in good agreement with experimental results. Initially using the plastic CTOD [9–12] and then the cyclic plastic strain itself [13][14], in a node release numeric model. This approach shown to effectively quantify the effects of ΔK [13], maximum and minimum loads [15], stress ratio, variable amplitude load patterns [16] and overloads [17]. Despite the promising results several limitations were found. Accordingly, in some cases the stress ratio effect was lower than expected [17] and the slopes of the numerical *da/dN*-ΔK curves were lower than the experimental ones [13,14]. These limitations indicate the need of additional mechanisms to fully characterize FCG.
A step towards solving this issue was the application of the GTN damage model, introducing porous damage effect in the existing node release model [18]. While the cyclic plastic strain at the crack tip remained as FCG driving force, porous damage shown to influence the stress state and plastic strain at the crack tip, as well as crack closure itself [19]. This was a demonstration of the interdependency of mechanisms that characterizes the fatigue phenomenon. From this perspective the main objective of this work is to provide a clear picture of the interactions between crack tip plastic strain, porous damage and crack closure. These interactions are

supposed to be reflected in the *da/dN*-Δ*K* results, which are compared to experimentally obtained ones.

2. NUMERICAL MODEL

All the numerical simulations employed in this study were conducted with the in-house finite element code DD3Imp [20][21]. An updated Lagrangian scheme is used to describe the evolution of the deformation process. The mechanical model assumes the elastic strains to be negligibly small with respect to unity and considers large elastoplastic strains and rotations.

2.1. Elasto-Plastic behaviour

The elasto-plastic behaviour of the 2024-T351 aluminium alloy is described through a phenomenological law. The isotropic elastic behaviour is modelled with Hooke´s law, where the Young modulus is affected by porosity:

$$E = (1 - f) \cdot E_0 \tag{1}$$

where E_0 is the void free material Young modulus and f the porosity. The yielding of the void free matrix is controlled by the von Mises criterion, where the equivalent stress is given by

$$\bar{\sigma} = \sqrt{\frac{3}{2}\boldsymbol{\sigma}' : \boldsymbol{\sigma}'}\ , \tag{2}$$

where $\boldsymbol{\sigma}'$ is the deviatoric stress tensor. The evolution of the yield surface is described by the combination of Swift and Lemaitre-Chaboche hardening laws, given by

$$\sigma_{\mathrm{y}} = k\left(\left(\frac{Y_0}{k}\right)^{\frac{1}{n}} + \bar{\varepsilon}^p\right)^n \tag{3}$$

$$\dot{\boldsymbol{X}} = C_{\mathrm{X}}\left[\frac{X_{\mathrm{sat}}}{\bar{\sigma}}(\boldsymbol{\sigma}' - \boldsymbol{X})\right]\dot{\bar{\varepsilon}}^{\mathrm{p}} with\ \dot{\boldsymbol{X}}(0) = 0, \tag{4}$$

In the case of the Swift law: Y_0, k, and n are the material parameters and $\bar{\varepsilon}^{\mathrm{p}}$ is the equivalent plastic strain. In the case of Armstrong-Frederick: $\boldsymbol{X}$ is the back stress tensor, X_{Sat} and C_{x} are material parameters and $\dot{\bar{\varepsilon}}^{\mathrm{p}}$ is the equivalent plastic strain rate. The material parameters are listed in Table 1 [21].

Table 1. Elastic properties and Swift and Lemaitre-Chaboche laws parameters obtained for the 2024-T351 aluminium alloy.

Material	E **(GPa)**	v **(-)**	Y_0 **(MPa)**	k **(MPa)**	n **(-)**	X_{Sat} **(MPa)**	C_X **(-)**
AA2024-T351	72.26	0.29	288.96	389.0	0.056	111.84	138.80

2.3. GTN damage model

The GTN model was based on the Gurson's yield surface [22], which considers materials to contain either cylindrical or spherical voids. The matrix is assumed free of voids and obeys the pressure insensitive von Mises yield criterion, equation (2). The initial yield surface was modified by Tvergaard [23] resulting in:

$$\phi = \left(\frac{\bar{\sigma}^2}{\sigma_{\mathrm{y}}}\right)^2 + 2q_1 f\cosh\left(q_2\frac{\mathrm{tr}\,\boldsymbol{\sigma}}{2\sigma_{\mathrm{y}}}\right) - 1 - q_3 f^2 \tag{5}$$

where f is the void volume fraction, tr $\boldsymbol{\sigma}$ the trace of the stress tensor, while q_1, q_2 and q_3 the Tvergaard void interaction parameters. This yield surface becomes pressure sensitive by considering a flow rule [24]:

$$\dot{\boldsymbol{\varepsilon}}^{\mathrm{p}} = \dot{\gamma}\frac{\partial\phi}{\partial\boldsymbol{\sigma}} = \dot{\gamma}\boldsymbol{\sigma}' + \frac{1}{3}\dot{\gamma}f\sigma_{\mathrm{y}}\sinh\left(\frac{3p}{2\sigma_{\mathrm{y}}}\right)\boldsymbol{I} \tag{6}$$

where $\dot{\gamma}$ is the plastic multiplier, p the hydrostatic-pressure and $\boldsymbol{I}$ the identity matrix [25]. The evolution of porosity, $\dot{f}$, is given by

$$\dot{f} = (f - f^2)\dot{\gamma}\sigma_{\mathrm{y}}\,sinh\left(\frac{3p}{2\sigma_{\mathrm{y}}}\right) + \frac{f_N}{s_N\sqrt{2\pi}}exp\left[-\frac{1}{2}\left(\frac{\bar{\varepsilon}^n - \varepsilon_N}{s_N}\right)^2\right]\dot{\bar{\varepsilon}}^p \tag{7}$$

where the GTN's nucleation law follows the Chu and Needleman [26] statistical model considering a Gaussian distribution with a mean plastic strain, ε_N, a standard deviation, s_N, and a maximum nucleation amplitude, f_N. The parameters for the GTN damage model were obtained from literature [27] and are listed in Table 2. Note that void coalescence is not modelled.

Table 2. GTN parameters adopted in the numerical model.

Material	f_0	q_1	q_2	q_3	f_N	ε_N	s_N
AA2024-T351	0.007	1.5	1	2.25	0.032	0.152	0.341

2.4. Geometry, mesh and loading case

A CT specimen, in accordance with the ASTM [28], is considered in Mode I [29]. Only the upper part of the specimen was modelled, to reduce computational cost, taking advantage of the existing symmetry. The constant amplitude cyclic load ranging between F_{min}=41.67 N/mm and F_{max}=416.7 N/mm results in a stress ratio, R=0.1. The CT specimen was discretized with 7287, 4-node, 2D plane strain finite elements and 7459 nodes. The region surrounding the crack path is meshed with elements of 8 μm, which allow to accurately evaluate the strong gradients of stresses and strains at this zone [30]. To reduce the computation cost, the outer region was coarser meshed. The experimental results were obtained in CT specimens with a thickness of 12 mm, therefore only plane strain conditions were applied.

2.5. Crack Propagation Strategy

A node release strategy [13] is used to model the FCG process. Accordingly, the crack advances 8 μm when the

plastic strain at the tip node reaches a critical value, ε_c^p, which is supposed to be a material property. The plastic strain is measured at the Gauss points and averaged at the node containing the crack tip. The FCG rate is obtained from the ratio between the crack increment (8 μm, which is the element size) and the number of load cycles, ΔN, required to reach the release criterion:

$$\frac{da}{dN} = \frac{8}{\Delta N} \quad (8)$$

A total plastic strain (TPS) approach was followed, which means that the plastic strain, and porosity, accumulated in the previous load cycles, at a certain node are not reset when propagation occurs. The FCG rate is assumed constant between crack increments as the crack propagation rate is usually relatively low (<1 μm/cycle). The numerical analysis of the crack growth is simplified by considering different sizes, a_0, for the initial straight crack. This allows to evaluate relatively wide ranges of ΔK with the same loading case. Moreover, the ΔK parameter is here strictly used to ease result comparison, ceasing the SSY requirement. FCG is only evaluated after some crack propagation which are required to stabilize the cyclic plastic deformation and the crack closure level. Finally, the contact between the flanks of the crack is modelled considering a rigid plane surface aligned with the crack symmetry plane.

3. RESULTS

Figure 1 presents the *da/dN*-ΔK curves predicted by the models with and without GTN. Both axes are displayed in *log-log* scales. The analysed initial crack sizes result in a ΔK variation between 7.86 and 15.5 MPa.m$^{0.5}$, which covers a significative part of the experimental data. The upper part of the experimental data refers to a regime close to ductile fracture. In this regime, the numerical data provides very high propagation rates, which cannot be analysed with the adopted mesh. The calibration provided a critical cumulative plastic strain for the model with GTN of 270% and for the version without GTN of 180%. The lines, presented in the right corner, indicate that the slope of the curve with GTN induces a much better approximation to the experimental results. As expected, for higher ΔK values the GTN model provides higher FCG rates, in comparison to the version without porous damage, allowing results in very good agreement with the experimental ones. This occurs because the introduction of porosity influences the stress-strain equilibrium, inducing higher levels of plastic strain. On the other hand, for the smaller initial crack size, the higher FCG rate is attained with the model without GTN, indicating an effect of the referred interrelation between mechanisms at the crack tip.

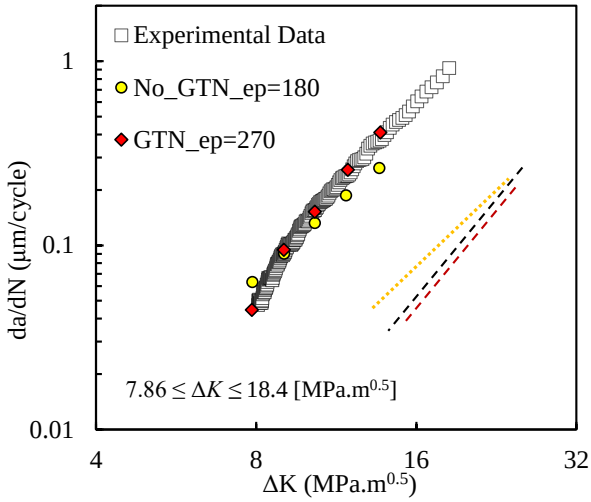

Figure 1. Comparison between experimental and numerical da/dN-ΔK curves, with and without GTN.

To understand the obtained FCG rate, the plastic strain accumulation was studied, for a_0=*11.5* and 16.5 mm, with and without GTN. The results are presented in terms of the pseudo-time (Figure 2 and Figure 3). Accordingly, the previous node release occurs at t-t_0=0s, plastic strain then accumulates, due to the load cycles, until another propagation occurs. Since the *da/dN* has a transient behaviour, thus the study falls on propagations on the stable *da/dN* zone. The ΔK level, corresponding to the crack size, at each propagation, is also shown in the figures. Remnants of the previous and following propagations are presented to highlight the cyclic behaviour of the plastic strain accumulation. The first studied propagation refers to a_0=11.5 mm, where *da/dN* is higher without GTN, and is presented in Figure 2. The critical plastic strain is achieved faster without GTN explaining the *da/dN* obtained for this ΔK (Figure 1).

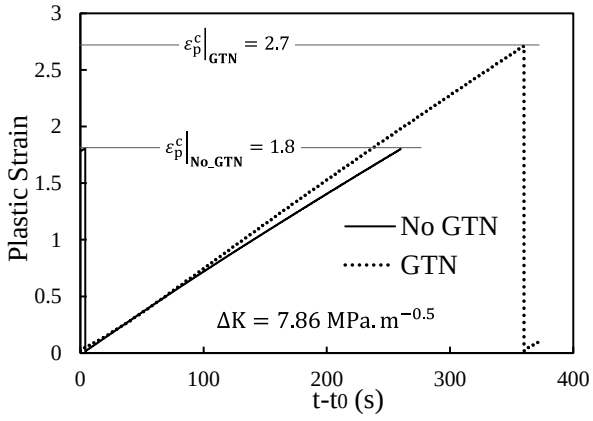

Figure 2. Plastic strain accumulation vs the load cycles that compose a single propagation, for a_0=11.5 mm.

Similar results, to the ones discussed before, are presented in Figure 3. However, here it refers to a_0=16.5 mm, an initial crack size where *da/dN* is higher with

GTN. Contrarily to the smaller initial crack size, the plastic strain accumulation is faster with the model with GTN, once again explaining the results obtained in Figure 1. Note that the effect of the porosity inclusion is such that the critical plastic strain for the model with GTN, is achieved faster that one in the version without GTN. The inversion on the behaviour of the plastic strain accumulation evidences the effect of additional mechanisms at the crack tip.

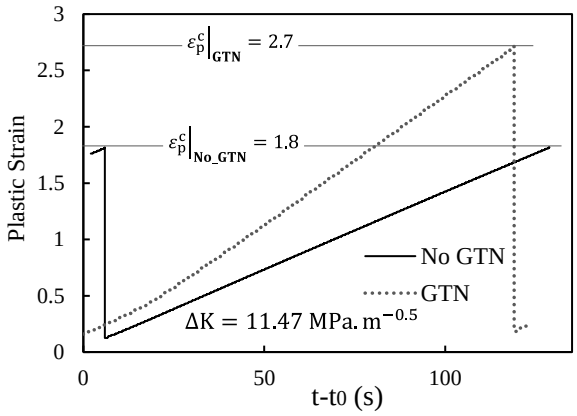

Figure 3. Plastic strain evolution for a_0=16.5 mm in the models with and without GTN.

The first mechanism analysed to explain the inversion on the plastic strain accumulation was crack closure. It is evaluated through the load cycles that compose the previously studied propagations, given by:

$$U^* = \frac{F_{open} - F_{min}}{F_{max} - F_{min}}, \quad (9)$$

where F_{open} is the crack opening load, F_{min} is the minimum load and F_{max} is the maximum load. The U^* parameter quantifies the fraction of load cycle during which the crack is closed. Crack closure is presented versus the fraction of the load cycles required to achieve the critical plastic strain. This allows comparison between results referring to different crack sizes. Figure 4 presents the crack closure evolution, with and without GTN, for a_0=11.5 mm, at ΔK=7.86 MPa.m$^{0.5}$. Considering the model without GTN, the crack closure is higher in the first load cycle (after the previous propagation) and decays rapidly due to strain ratcheting, vanishing after some load cycles. On the other hand, in the model with GTN, crack closure maintains a relatively high level, protecting the material since it reduces the effective intensity of the stress state acting at the crack tip. The higher crack closure level on the model with GTN is explained by the higher plastic strains achieved in this version of the model, which stimulates Plastic Induced Crack Closure. Additionally, the inclusion of porosity increases the volume of the deformed material at the crack flanks increasing the contact between them. This indicates that crack closure is to blame for the FCG rate obtained for this ΔK level.

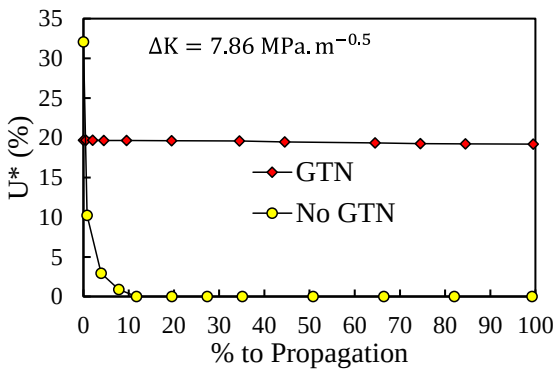

Figure 4. Crack closure evolution, through the load cycles that compose a propagation, for a_0=11.5 mm.

The crack closure evolution was also studied for a_0=16.5 mm, with the results being presented in Figure 5. Once again crack closure has a peak in the first loading cycle, decaying rapidly in the version without GTN. However, in this case crack closure is always higher in the model with GTN, due to the same reasons discussed above. Besides, it also presents an initial peak, decaying with the accumulation of load cycles but, in this version, it never ceases, keeping a level even higher than the one verified for ΔK=7.86 MPa.m$^{0.5}$. For some reason, for higher ΔK levels crack closure is not able to fully protect the material, despite its high level. Thus, another mechanism should interfere in FCG for ΔK values above 10.36 MPa.m$^{0.5}$.

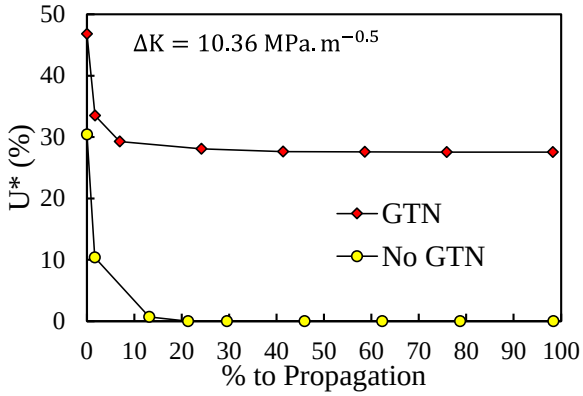

Figure 5. Crack closure evolution, through the load cycles that compose a propagation, for a_0=16.5 mm.

The evolution of the porosity during a single propagation is presented in Figure 6 for the of initial crack length. Results show a higher porosity level for the higher initial crack size, as expected, due to the also harsher stress state achieved for ΔK=10.36 MPa.m$^{0.5}$. Note that there is a discharge of plastic strain after each propagation, as the crack tip moves further to a less plastically deformed zone. However, for a_0=16.5 mm, once the crack advances to the following node it finds a more strained zone in comparison with the case a_0=11.5 mm. This explains the higher plastic strain and porosity at the first load cycle for a_0=16.5 mm. Besides, porosity presents

distinct evolutions for both ΔK levels. Accordingly, for ΔK=7.86 MPa.m$^{0.5}$ porosity rises quickly and eventually saturates. On the other hand, for a_0=16.5 mm porosity gradually increases throughout all the propagation reaching higher levels. Thus, porous damage may explain the attained *da/dN* results. Accordingly, the higher porosity, achieved at a_0=16.5 mm, induces such harsh stress and strain states that counterbalance the protective effect of crack closure, generating higher plastic strain accumulation rates. These results show that stress triaxiality influences and is influenced by porosity, proofing that FCG is only explained considering the effect of each mechanism as a whole and not in isolation. Finally, note that porosity presents an oscillating behaviour, which is more relevant for the higher initial crack sizes. This occurs because on the unloading stage, stress state is majorly compressive, causing a collapse of the micro-voids. Due to entropy law, porous damage is of irreversible character, thus, during the loading phase the micro-voids reopen.

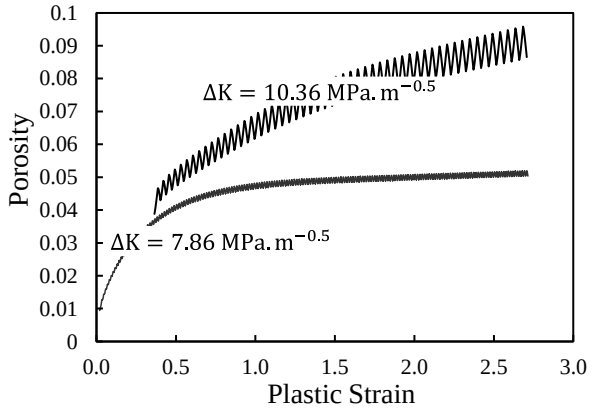

Figure 6. Porosity evolution at the crack tip due to the plastic strain accumulation for the two studied initial crack sizes.

4. CONCLUSION

In this work fatigue crack growth is studied with a node release numerical model considering the cyclic plastic strain at the crack tip to be the fatigue driving force. Porous damage is included through the introduction of the GTN damage model, which allows a much better approximation to the experimental results. The causes of this success were analysed and show to be related with the different mechanisms that act at the crack tip. Indeed, FCG is deeply influenced by the relations between porosity, plastic strain, crack closure and stress state, which controls the stress triaxiality at the crack tip. Moreover, to explain the attained results it is crucial to understand how these mechanisms relate with each other analysing them as a whole and not in isolation.

ACKNOWLEDGEMENTS

This research was funded by Portuguese Foundation for Science and Technology (FCT) under the project with reference PTDC/EME-EME/31657/2017 and by UIDB/00285/2020.

REFERENCES

[1] Campbell, J., Invisible macrodefects in castings, J. Phys. IV Fr. 03 (1993) C7-861-C7-872.

[2] H. Masuo, Y. Tanaka, S. Morokoshi, H. Yagura, T. Uchida, Y. Yamamoto, Y. Murakami, Influence of defects, surface roughness and HIP on the fatigue strength of Ti-6Al-4V manufactured by additive manufacturing, Int. J. Fatigue. 117 (2018) 163–179.

[3] P. Paris, F. Erdogan, A critical analysis of crack propagation laws, J. Basic Eng., Trans. ASME. 85 (1963) 528–533.

[4] C.T. Sun, Z.-H. Jin, Chapter 7 - Elastic-Plastic Fracture Criteria, in: C.T. Sun, Z.-H.B.T.-F.M. Jin (Eds.), Academic Press, Boston, 2012: pp. 171–187.

[5] A.P. Kfouri, Limitations On The Use Of The Stress Intensity Factor, K, As A Fracture Parameter In The Fatigue Propagation Of Short Cracks, Fatigue & Fract. Eng. Mater. & Struct. 20 (1997) 1687–1698.

[6] J. Tong, L.G. Zhao, B. Lin, Ratchetting strain as a driving force for fatigue crack growth, Int. J. Fatigue. 46 (2013) 49–57.

[7] H.-B. Park, K.-M. Kim, B.-W. Lee, Plastic zone size in fatigue cracking, Int. J. Press. Vessel. Pip. 68 (1996) 279–285.

[8] B. Ould Chikh, A. Imad, M. Benguediab, Influence of the cyclic plastic zone size on the propagation of the fatigue crack in case of 12NC6 steel, Comput. Mater. Sci. 43 (2008) 1010–1017.

[9] F. V Antunes, R. Branco, P.A. Prates, L. Borrego, Fatigue crack growth modelling based on CTOD for the 7050-T6 alloy, Fatigue Fract. Eng. Mater. Struct. 40 (2017) 1309–1320.

[10] F. V Antunes, S. Serrano, R. Branco, P. Prates, Fatigue crack growth in the 2050-T8 aluminium alloy, Int. J. Fatigue. 115 (2018) 79–88.

[11] F. V Antunes, M.S.C. Ferreira, R. Branco, P. Prates, C. Gardin, C. Sarrazin-Baudoux, Fatigue crack growth versus plastic CTOD in the 304L stainless steel, Eng. Fract. Mech. 214 (2019) 487–503.

[12] P. Prates, A. Marques, M. Borges, R. Branco, F. V Antunes, Numerical Study on the Variability of Plastic CTOD, Materials (Basel). 13 (2020) 1276.

[13] M. Borges, D.M. Neto, F. V Antunes, Numerical simulation of fatigue crack growth based on accumulated plastic strain, Theor. Appl. Fract. Mech. 108 (2020) 102676.

[14] F.F. Ferreira, D.M. Neto, J.S. Jesus, P.A. Prates, F. V Antunes, Numerical Prediction of the Fatigue Crack Growth Rate in SLM Ti-6Al-4V Based on Crack Tip Plastic Strain, Metals (Basel). 10 (2020).

[15] M.F. Borges, D.M. Neto, F. V Antunes, Revisiting Classical Issues of Fatigue Crack Growth Using a Non-Linear Approach., Mater. (Basel, Switzerland). 13 (2020).

[16] R.S. D.M. Neto, M.F. Borges, F.V. Antunes, Numerical analysis of Super Block 2020 loading sequence, Eng. Fract. Mech. (2020).

[17] D.M. Neto, M.F. Borges, F. V Antunes, J. Jesus, Mechanisms of fatigue crack growth in Ti-6Al-4V alloy subjected to single overloads, Theor. Appl. Fract. Mech. 114 (2021) 103024.

[18] E.R. Sérgio, F. V Antunes, M.F. Borges, D.M. Neto, FCG modelling considering the combined effects of cyclic plastic deformation and growth of micro-voids, Materials (Basel). (2021) 1–18.

[19] E.R. Sérgio, F. V Antunes, D.M. Neto, M.F. Borges, Study on the Influence of the Gurson–Tvergaard–Needleman Damage Model on the Fatigue Crack Growth Rate, Metals (Basel). 11 (2021).

[20] L.F. Menezes, C. Teodosiu, Three-dimensional numerical simulation of the deep-drawing process using solid finite elements, J. Mater. Process. Technol. 97 (2000) 100–106.

[21] M.C. Oliveira, J.L. Alves, L.F. Menezes, Algorithms and Strategies for Treatment of Large Deformation Frictional Contact in the Numerical Simulation of Deep Drawing Process, Arch. Comput. Methods Eng. 15 (2008) 113–162.

[22] A.L. Gurson, Continuum Theory of Ductile Rupture by Void Nucleation and Growth: Part I—Yield Criteria and Flow Rules for Porous Ductile Media, J. Eng. Mater. Technol. 99 (1977) 2–15.

[23] V. Tvergaard, Influence of voids on shear band instabilities under plane strain conditions, Int. J. Fract. 17 (1981) 389–407.

[24] J. Brito, Ductile fracture prediction using a coupled damage model, in: 2018.

[25] L. Malcher, Continuum Modelling and Numerical Simulation of Damage for Ductile Materials, Fac. Eng. Univ. Do Porto. (2012).

[26] C.C. Chu, A. Needleman, Void Nucleation Effects in Biaxially Stretched Sheets, J. Eng. Mater. Technol. 102 (1980) 249–256.

[27] D. Chen, Y. Li, X. Yang, W. Jiang, L. Guan, Efficient parameters identification of a modified GTN model of ductile fracture using machine learning, Eng. Fract. Mech. 245 (2021) 107535.

[28] ASTM E 647-15: Standard test method for measurement of fatigue crack growth rates. Philadelphia: American Society for Testing and Materials (2015) ASTM.

[29] M. Borges, P. Lopez-Crespo, F. V Antunes, B. Moreno, P. Prates, D. Camas, D.M. Neto, Fatigue crack propagation analysis in 2024-T351 aluminium alloy using nonlinear parameters, Int. J. Fatigue. 153 (2021) 106478.

[30] F. V Antunes, D. Camas, L. Correia, R. Branco, Finite element meshes for optimal modelling of plasticity induced crack closure, Eng. Fract. Mech. 142 (2015) 184–200.